Antenna Characteristics and Air-Ground Interface Deembedding Methods for Stepped-Frequency Ground Penetrating Radar Measurements

Brian Karlsen[ab], Jan Larsen[a], Kaj B. Jakobsen[b], Helge B.D. Sørensen[b], Staffan Abrahamson[c]

[a]Department of Mathematical Modelling, Technical University of Denmark
Richard Petersens Plads, Building 321, DK-2800 Kongens Lyngby, Denmark

[b]Department of Applied Electronics, Technical University of Denmark
Akademivej, Building 451, DK-2800 Kongens Lyngby, Denmark

[c]Division of Sensor Technology, National Defense Research Establishment (FOA)
P.O. Box 1165 S-581 11, Linköping, Sweden

ABSTRACT

The result from field-tests using a Stepped-Frequency Ground Penetrating Radar (SF-GPR) and promising antenna and air-ground deembedding methods for a SF-GPR is presented. A monostatic S-band rectangular waveguide antenna was used in the field-tests. The advantages of the SF-GPR, e.g., amplitude and phase information in the SF-GPR signal, is used to deembed the characteristics of the antenna. We propose a new air-to-ground interface deembedding technique based on Principal Component Analysis which enables enhancement of the SF-GPR signal from buried objects, e.g., anti-personal landmines. The methods are successfully evaluated on field-test data obtained from measurements on a large-scale in-door test field.

Keywords: Anti-personal mine detection, stepped-frequency GPR, antenna deembedding, air-to-ground interface deembedding, principal component analysis

1. INTRODUCTION

Landmines, especially anti-personal landmines (APL) pose a significant problem of global proportions. A previously estimated number of buried landmines world-wide, was as many as $80 - 110$ millions. The problem is especially a growing threat both to the military forces and to the lives, limbs, and economic welfare of civilians in the war-torn and the developing countries. International consensus has been established to reduce the world-wide landmine problem, by banning the use of landmines and neutralize mine fields. However, the detection problem has becomes extremely hard since mines have been reduced in size, and furthermore, due to the fact that most modern APL's are based mainly on non-metallic substances.

Our objective is to identify small mine-shaped metallic and non-metallic objects buried in the ground using a GPR. The most widely used GPRs are: the pulse radar, the Frequency-Modulated-Continuous-Wave (FW-CW) radar, and the Stepped-Frequency (SF) radar. Our research and experiments are based on the SF-GPR approach. The used antenna of the SF-GPR was an open-ended wave guide operating in the S-band.[7–9] The SF-GPR approach is chosen due to its advantages of measuring both the amplitude and phase information of the SF-GPR signal, and the advantages regarding pulse modulation.

So far, promising results have been obtained using a GPR. However, detecting small non-metallic mines is still of major concern. GPR signals from mines of plastic is in general very small, due to the fact that plastic have similar electromagnetic properties as ordinary types of soil. In order to enhance detection of non-metallic mines, unwanted GPR signal components needs to be reduced. This cover e.g., the antenna characteristics and the air-to-ground impulse response.

Additional author information. it BK: bka@eivind.imm.dtu.dk, eivind.imm.dtu.dk; *JL*: jl@imm.dtu.dk, eivind.imm.dtu.dk; *KBJ*: kbj@iae.dtu.dk, www.iae.dtu.dk; *HBDS*: hbs@iae.dtu.dk, www.iae.dtu.dk; *SA*: staabr@lin.foa.se, www.foa.se

In Section 3 a new approach for deembedding of the antenna characteristic is presented. The antenna deembedding approach deploy the advantages of SF-GPR. Section 4 presents a promising Principal Component Analysis (PCA) approach to deembed the air-to-ground impulse response.

2. THE FREQUENCY STEPPED RADAR AND MEASUREMENTS

The presented deembedding methods in this paper is evaluated on field-test data. The field test data were collected at large-scale indoor test facilities at FOA. Figure 1 shows an outline of the indoor measurement system shown. The measurement system consists of linear bearings where the antenna is mounted. The antenna can be moved in the x and y-directions down to steps of 10 mm. The position of the antenna is controlled by the PC via the step-motors and linear bearings. The antenna is connected via a 10 m long coaxial cable to a HP8753C network analyzer that is set up to measure the amplitude and phase of the reflection coefficient.

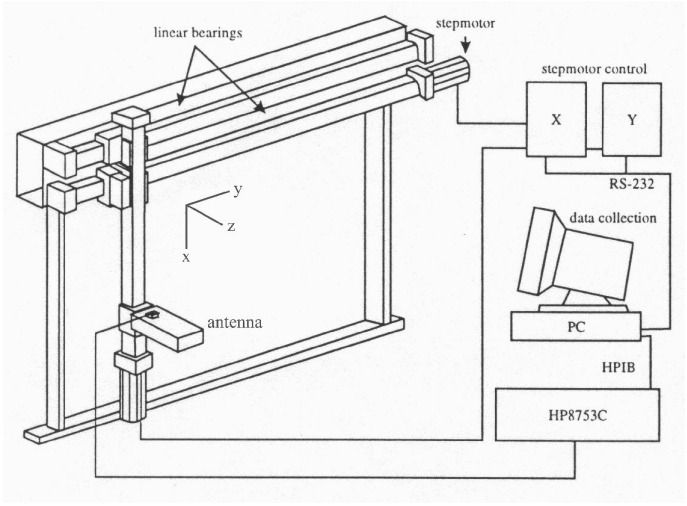

Figure 1. Outline of the indoor measurement facilities. The position of the antenna is controlled in x and y-direction by the PC via the step motors. The open end of the antenna is 17.5 cm above ground.

Figure 2 shows the coordinates in x, y, z given for each measurement setup. The mines considered is this study was a non-metallic M56 landmine filled with beeswax, and a M56 shaped dummy mines of iron. All the objects have the same irregular shape with a diameter of 5.4 cm and a height of 4.0 cm.

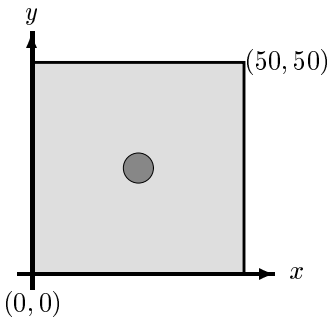

Object	M56 dummy	Iron
x-position (cm)	25	25
y-position (cm)	25	25
z-position, depth from surface (cm)	5	5

Figure 2. The mines considered is this study is a non-metallic M56 dummay landmine filled with beeswax, and a M56 shaped mine of iron. The black marks indicate a landmine. The corner-coordinates indicate the number of measurement points. The step-size is equal 1.0 cm in both directions, thus the field of view are 50 by 50 cm.

For all setup the antenna were stepped 1.0 cm in both x and y-directions. The open end of the waveguide antenna is elevated 17.5 cm above the ground and operates mainly in the far-field. The soil was sand with a relative permittivity $\epsilon_r \approx 3$ which is very close to that of the M56 dummy plastic mine. The network analyzer was setup to measure amplitude and phase of the reflection coefficient for 291 frequencies in range of $2.5 - 3.95$ GHz (frequency step 5 MHz.)

3. ANTENNA DEEMBEDDING

The received SF-GPR time-signal waveform can be described as the convolution of a number of time functions each representing the impulse response of the radar systems' components corrupted by noise from various sources. Hence, the received SF-GPR time-signal waveform $r(t)$ can be expressed as[1]

$$r(t) = s(t)*a_1(t)*c(t)*g_1(t)*o(t)*g_2(t)*a_2(t) + n(t) \tag{1}$$

where

- $s(t)$ is the signal applied to the antenna,
- $c(t)$ is the antenna cross coupling response,
- $a_i(t)$ are the antenna impulse response in forward and backward directions*, and
- $g_i(t)$ are ground impulse responses in forward and backward directions,
- $o(t)$ is the object impulse response.

The objective of the antenna deembedding is to deembed the characteristics of the antenna expressed by $a(t)$ in (1). The antenna deembedded signal may be expressed[1] as:

$$r'(t) = s(t)*c(t)*g(t)*o(t)*g(t) + n'(t) \tag{2}$$

Define $R(\omega)$ as the spectrum of r(t) where ω is the angular frequency. Further define $A_{12}(\omega)$ as the spectrum of $a_1(t) * a_2(t)$. Then the spectrum of the deembedded signal, $R'(\omega)$, can be written as $R'(\omega) = R(\omega)A_{12}^{-1}(\omega)$.

If the SF-GPR system is calibrated at the antenna connector input, the advantages of the SF-GPR makes it possible to perform antenna deembeeding using the amplitude and phase of the reflection coefficient at a number of frequency bins. The antenna responses given by $a_1(t)$ and $a_2(t)$ can be measured or simulated. The deployed S-band rectangular waveguide antenna[7–9] obey $A_{12}(\omega) \approx \exp(-j2\Theta(\omega))$ where $\Theta(\omega)$ is equal to the electrical length of the antenna. The electric length is measured by short circuiting the open end of the antenna. The approximation of $A_{12}(\omega)$ also accounts for the dispersion of the antenna.

In Figure 3 the result of the antenna deembedding is shown for a one 1-dimensional SF-GPR scan in a location without mines. The left plot show the received time-signal waveform before antenna deembedding ($r(t)$) and the right plot show the received time-signal waveform after antenna deembedding ($r'(t)$). Both signals are generated from the measured SF-GPR spectrum by the following steps: 1) the spectrum is weighted by a Kaiser window[6] of length 291 with parameter 2π to suppress edge effects. 2) Next, the spectrum is padded with zeros to obtain a sampling frequency of $f_s = 10.23$ Ghz. 3) Finally, the inverse Fast Fourier Transform is applied to obtain the time signals. The dashed lines correspond to the ground surface. In the right plot the ground surface reflection is noticed at 1.2 nsec, which correspond to the distance from antenna to the ground, i.e., 17.5 cm.

*In our case the antenna is monostatic, i.e., $a_1(t) = a_2(t)$.

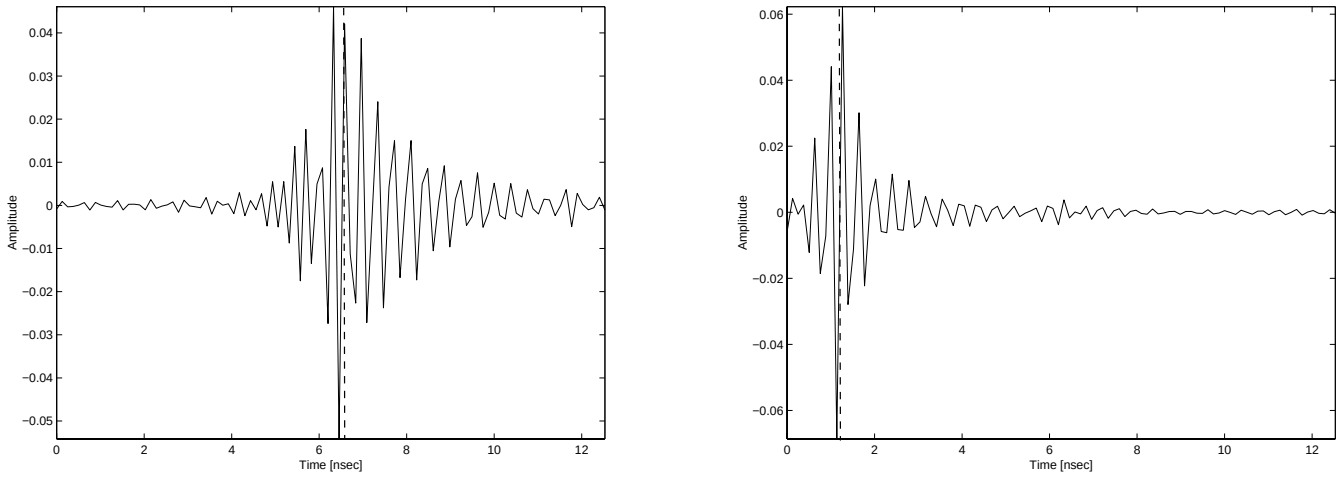

Figure 3. *Left*: Received time-signal before antenna deembedding ($r(t)$). *Right*: Received time-signal after antenna deembedding ($r'(t)$). The dashed lines correspond to the ground surface. The ground surface reflection is located at 1.2 nsec, corresponding to the distance from antenna to the ground, i.e., 17.5 cm. Further, notice that the deembedded signal has a much more narrow response which enhances the resolution of SF-GPR time signal.

4. AIR-TO-GROUND DEEMBEDDING

Let $s_{ij}(t)$ denote the signal received at location $x = (i-1)$ cm, $y = (j-1)$ cm, where $i = 1, 2, \cdots, I$ and $j = 1, 2, \cdots, J$. Traditional air-to-ground deembedding[1] consists in subtracting the mean scan across the xy-plane, i.e.,

$$\bar{s}_{ij}(t) = s_{ij}(t) - \frac{1}{IJ}\sum_{i=1}^{I}\sum_{j=1}^{J} s_{ij}(t) \tag{3}$$

This procedure removes the common signal across the xy-plane which is mainly believed to originate from the very strong air-to-ground reflection. However, this approach is often insufficient to enhance the signature from mine-like objects due to variation in the ground surface and inhomogeneities in the soil. A novel approach based on Principal Component Analysis (PCA) and the closely related Singular Value Decomposition (SVD) is suggested. PCA is very well-suited for high-dimensional, highly correlated data. PCA analysis has previously been applied to GPR data analysis in[10] for detection of mines on preprocessed data using cross track-depth scans (xz-plane images). The approach taken here is different and inspired by explorative analysis of functional neuroimages.[2,5]

Define the $P \times N$ signal matrix

$$\boldsymbol{S} = \{S_{p,t}\}, \quad S_{p,t} = \bar{s}_{i,j}(t), \; p = i + (j-1)\cdot I, \; i \in [1; I], \; j \in [1; J] \tag{4}$$

where the pixel index $p \in [1; P]$, $P = I \cdot J$, and the time index $t \in [1; N]$ with N being the total number of time samples. Column t of the matrix then represent the xy-plane scan image at time t, reshaped into a vector. The signal matrix thus represents the sequence of xy-plane images along the time or z-direction. Usually $P \gg N$, in our case $P = 51^2 = 2601$ and $N = 40$.

Since the rank of $\boldsymbol{S}$ is at most N, the SVD of $\boldsymbol{S}$ reads

$$\boldsymbol{S} = \boldsymbol{U}\boldsymbol{D}\boldsymbol{V}^\top = \sum_{i=1}^{N} \boldsymbol{u}_i D_{i,i} \boldsymbol{v}_i^\top, \qquad S_{p,t} = \sum_{i=1}^{N} U_{p,i} D_{i,i} V_{t,i} \tag{5}$$

where the $P \times N$ matrix $\boldsymbol{U} = \{U_{p,i}\} = [\boldsymbol{u}_1, \boldsymbol{u}_2, \cdots, \boldsymbol{u}_N]$ and the $N \times N$ matrix $\boldsymbol{V} = \{V_{t,i}\} = [\boldsymbol{v}_1, \boldsymbol{v}_2, \cdots, \boldsymbol{v}_N]$ represent the orthonormal basis vectors[†], i.e., eigenvectors of the symmetric matrices $\boldsymbol{S}\boldsymbol{S}^\top$ and $\boldsymbol{S}^\top\boldsymbol{S}$, respectively.

[†]That is, $\boldsymbol{U}^\top\boldsymbol{U} = \boldsymbol{I}$ and $\boldsymbol{V}^\top\boldsymbol{V} = \boldsymbol{I}$, where $\boldsymbol{I}$ is the identity matrix.

$\boldsymbol{D} = \{D_{i,i}\}$ is a $N \times N$ diagonal matrix of singular values ranked in decreasing order, as shown by $D_{i-1,i-1} \geq D_{i,i}$, $\forall\, i \in [2; N]$. The SVD identifies a a set of uncorrelated time sequences, the Principal Components (PC's): $\boldsymbol{y}_i = D_{i,i}\boldsymbol{v}_i$, enumerated by the component index $i = 1, 2, \ldots, N$ and $\boldsymbol{y}_i = [y_i(1), \cdots, y_i(N)]^\top$. That is, we can write the observed signal matrix (image sequence) as a weighted sum of fixed eigenvectors (eigenimages) $\boldsymbol{u}_i$ that often lend themselves to direct interpretation. The i'th PC constitutes the normalized linear combination of pixel components with maximum variance under the constraint that it is orthogonal to other PC's, i.e., $\boldsymbol{y}_i^\top \boldsymbol{y}_k = 0$, $\forall\, k \neq i$. The variance of $\boldsymbol{y}_i^\top$ is $D_{i,i}^2$.

Consider the projection onto the subspace spanned by the first M PC's, i.e.,

$$\boldsymbol{Y} = \widetilde{\boldsymbol{U}}^\top \boldsymbol{S}, \quad \widetilde{\boldsymbol{U}} = [\boldsymbol{u}_1, \boldsymbol{u}_2, \cdots, \boldsymbol{u}_M] \tag{6}$$

where $\boldsymbol{Y}$ is an $M \times N$ matrix. This provides explanation of

$$\delta = 100\% \cdot \sum_{i=1}^{M} D_{i,i}^2 \cdot \left(\sum_{i=1}^{N} D_{i,i}^2 \right)^{-1} \tag{7}$$

of the total variance in $\boldsymbol{S}$. That is, $\boldsymbol{S}$ can be reconstructed optimally (in mean square error sense) from the subspace via

$$\widehat{\boldsymbol{S}} = \widetilde{\boldsymbol{U}}\boldsymbol{Y} \tag{8}$$

4.1. Mean Value Deembedding

The traditional deembedding by subtracting the mean scan across the xy-plane according to (3) is shown in Figures 4 and 5, for the metal and M56 dummy mine recordings described in Figure 2. $I, J = 51$ corresponds to an area of $50 \times 50\,\mathrm{cm}$, and $N = 40$ to a depth of maximum 3.91 ns. The figures show power of the signals estimated using a length 3 non-causal Kaiser window[6] with parameter 2π. All images in a time sequence are scaled individually using 64 gray-values. This is motivated by the fact that detection of unknown mines would proceed from thresholding the top 5% values, say. It is noticed that images up to time approximately $t = 17$ are dominated by the air-to-ground reflection. In the later images the metal mine is noticed, however, using the above mentioned threshold technique result in numerous false alarms. In the mean subtracted case, the air-to-ground disturbance is reduced, however, still clutter will produce false alarms. As expected, plastic mines are much harder to detect than metal mines, since the reflections are very small.

4.2. PCA based Deembedding

SVD is deployed on the signal matrix $\boldsymbol{S}$ as described above. Using an explanation coefficient $\delta = 99.9\%$ (see (7)) provides a relatively small number of principal components (PC's) and associated eigenimages. Each eigenimage summarizes the reflections associated with the time signature given by the corresponding PC time signal. Figures 6 and 7 display the power of the PC signals[‡] and associated eigenimages. If the PC time signal is rather peaked, then the eigenimage corresponds to the reflection from the depth related to the peak location. Furthermore, the variance of the PC's decrease with the PC number, indicating the strength of the reflections from various depths.

Figures 8 and 9 show comparison between the previous mentioned mean subtraction method and the PCA based reconstruction of the signal matrix. PCA reconstruction is done using (8) from a set of selected PC's. The PC's corresponding to the air-to-ground reflections are omitted when performing the reconstruction. For the metal mine PC1 is omitted, whereas PC1 and PC2 are omitted in the M56 dummy mine case.

[‡]The power is, as earlier, calculated using a non-causal Kaiser window of size 3 with and characteristic parameter 2π.

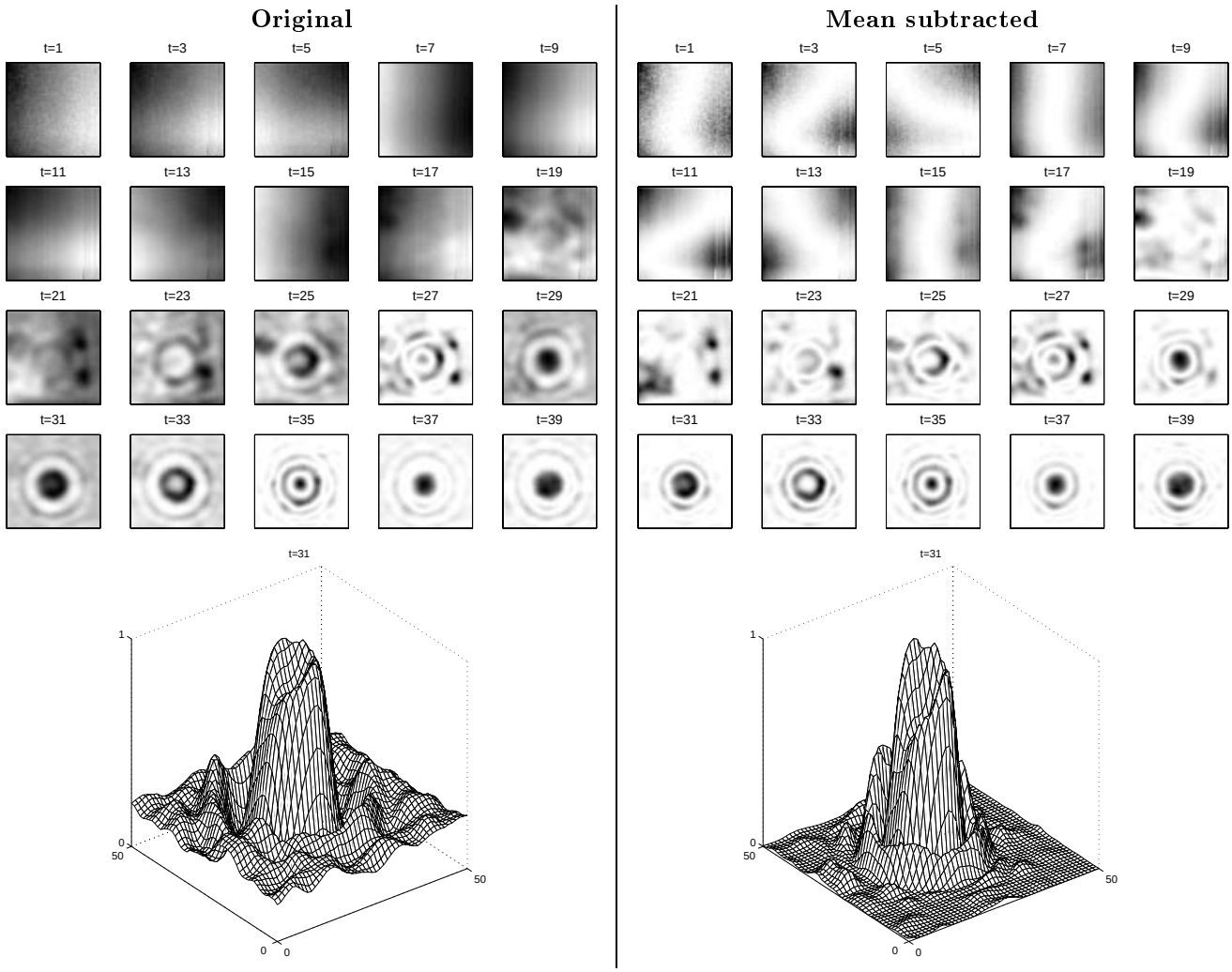

Figure 4. *Metal mine*: The flat images depicts the power of the original received signals in the xy-plane for various time steps t. Left panel show the original signals whereas the right panel show the mean subtracted signals. All images in a time sequence are scaled individually for optimal use of the available 64 gray-values. Images up to time approximately $t = 17$ are dominated by the air-to-ground reflection. In the later images the metal mine is noticed. Using the mean subtracted image clearly reduce clutter and number of false alarms. The mesh plots further demonstrate the reduction of clutter in the mean subtracted case.

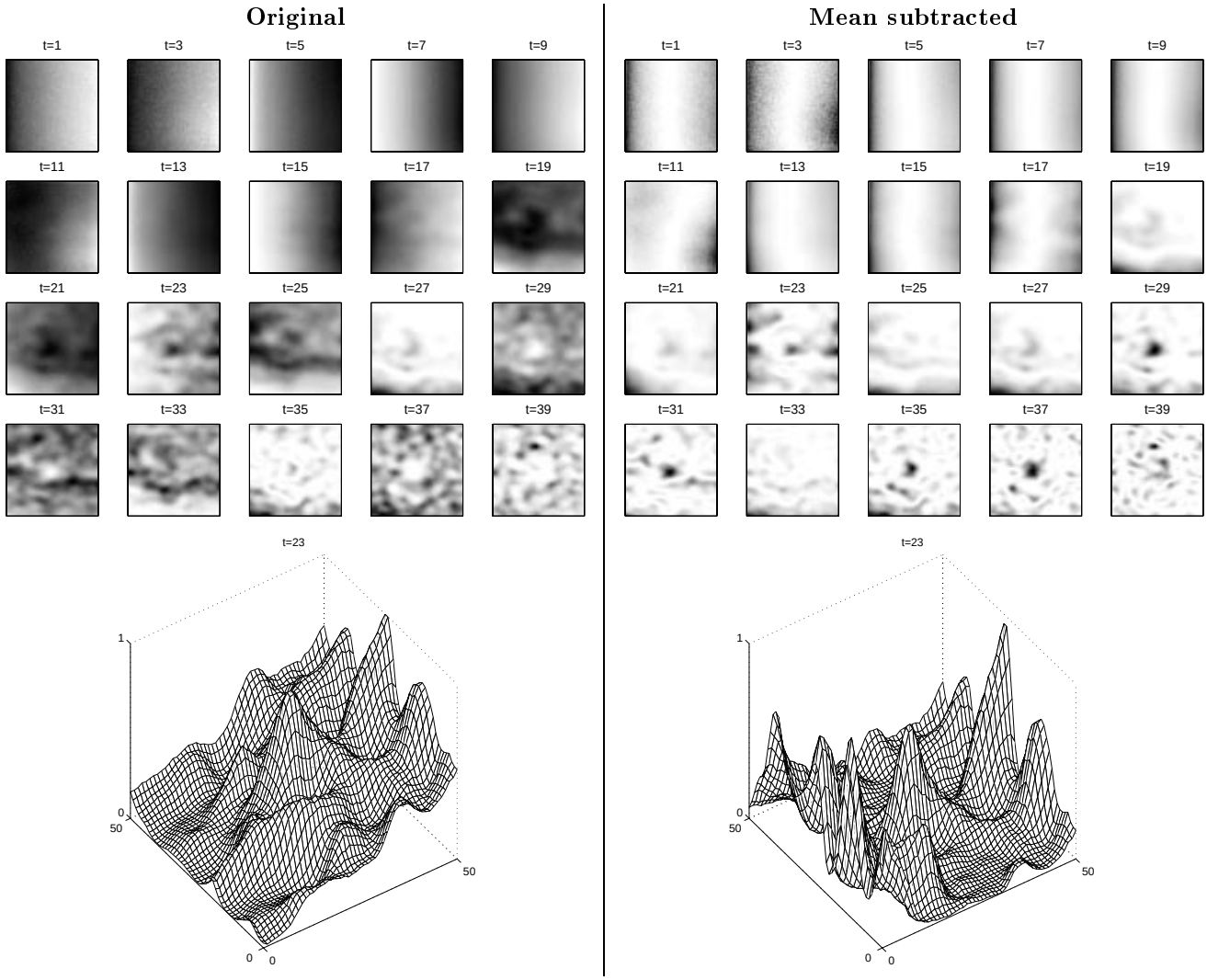

Figure 5. *M56 dummy mine*: The comments made about the metal mine case also applies for the plastic dummy mine. However, clearly the signal from the plastic mine is less pronounced causing clutter to be even more annoying.

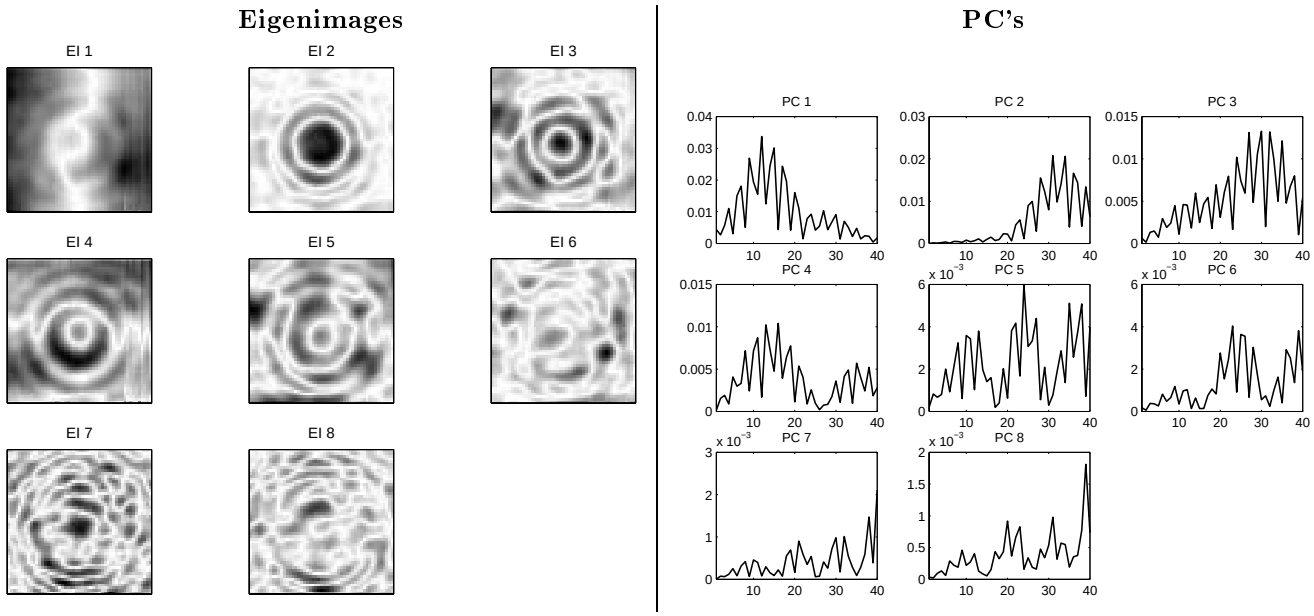

Figure 6. *Metal mine*: The left panel shows the eigenimages (in xy-plane) and the right panel the associated principal components (PC's). PC1 shows a peak close to the air-to-ground interface, and the associated eigenimage provides the fluctuation in the almost planar ground. PC2 peak much later and the associated eigenimage clearly has strong mine signature. Subsequent PC's become less focused in time and the eigenimages show a clutter like texture. Also notice that the power of the PC's decrease with the number, indicating that the air-to-ground reflection has the strongest power, the mine signal has smaller power, and clutter has lowest power.

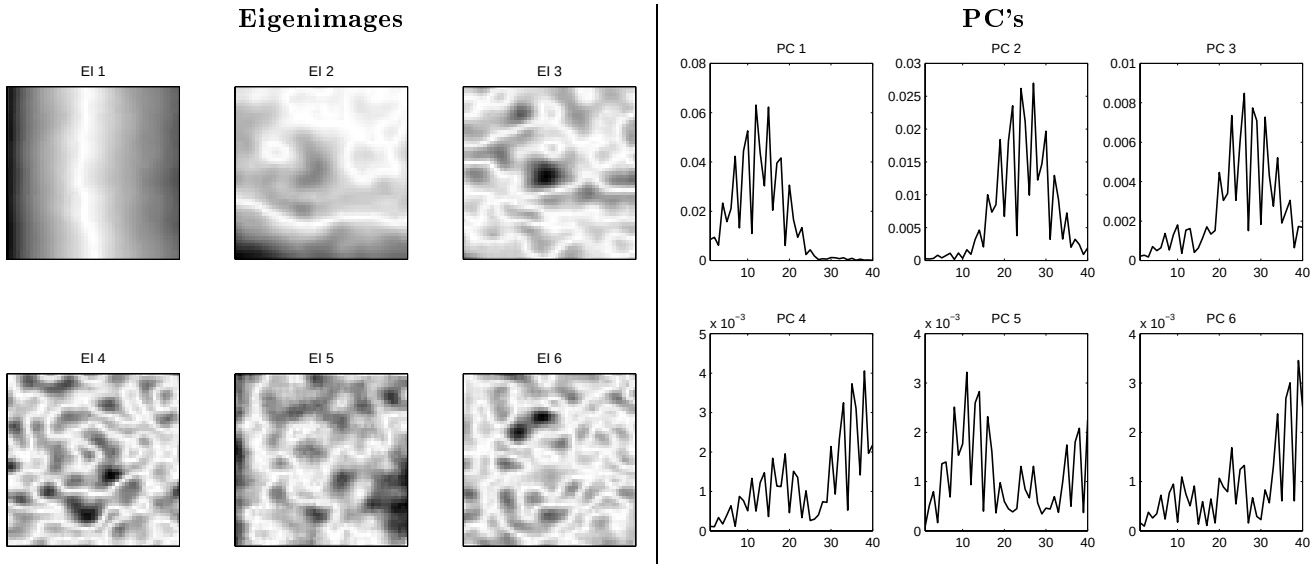

Figure 7. *M56 dummy mine*: The left panel shows the eigenimages (in xy-plane) and the right panel the associated principal components (PC's). PC1 shows as in the metal mine case a peak close to the air-to-ground interface and the associated eigenimage provides the fluctuation in the almost planar ground. In this case, the ground fluctuation is more pronounced, as seen both in the eigenimage and in the PC1 signature which is clearly more peaked. PC2 is rather broad thus the eigenimage shows both ground and mine signatures. PC3 is more peaked around the time corresponding to the mine z-location. In addition, the eigenimage shows a stronger mine like signature. The remaining components are more mixed clutter/mine signals, however, also they have much less power.

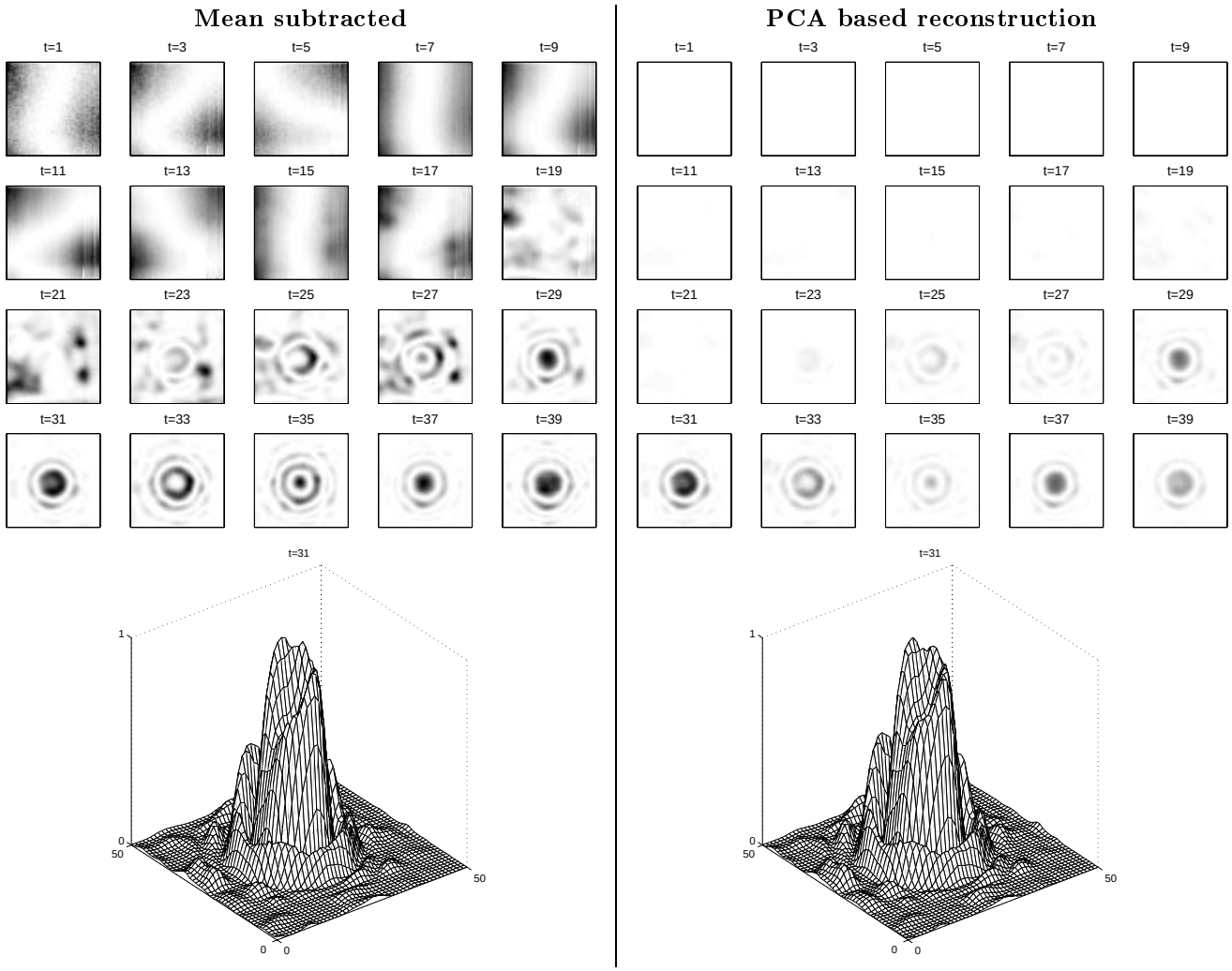

Figure 8. *Metal mine*: Left panel shows the result of the mean subtraction method and is identical to that of Figure 4. The right panel shows the result of the PCA based reconstruction of the signal matrix. Clearly, the air-to-ground disturbance is removed and the clutter significantly reduced. The images at $t = 31$ shows the strongest signature, and clearly represent the metal mine. The physical location of the mine corresponds approximately to $t = 18$. The seemingly dislocated mine signature at $t = 31$ is partly related to multiple reflections and partly to the fact that the radar cross-section is larger from oblique angles.

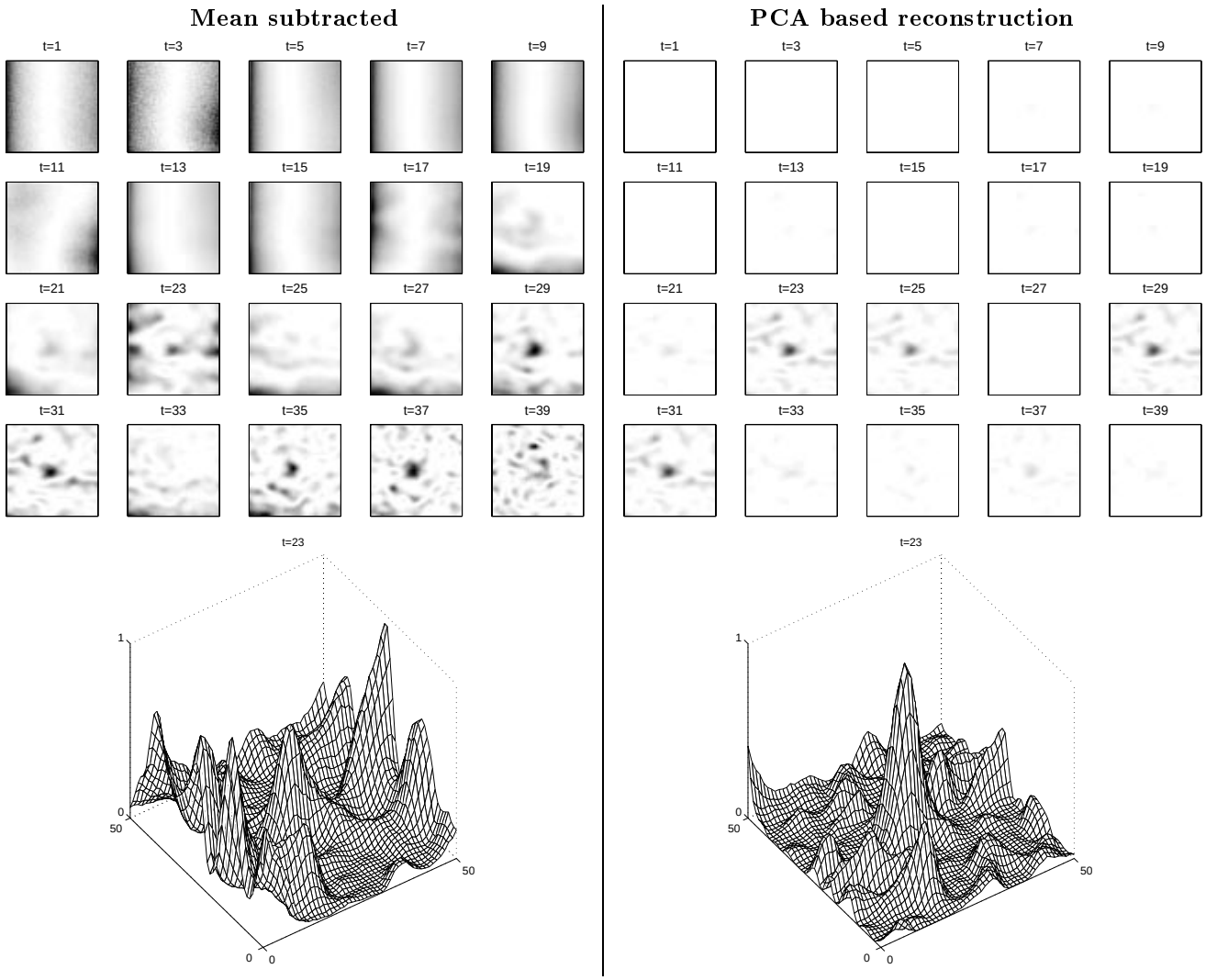

Figure 9. *M56 dummy mine*: Left panel shows the result of the mean subtraction method and is identical to that of Figure 5. The right panel shows the result of the PCA based reconstruction of the signal matrix. Like in the metal mine case, the air-to-ground disturbance is removed and the clutter significantly reduced. The PCA based images at $t = 23$ shows the strongest signature, and clearly represent the mine and is very close to the physical location of the mine at approximately $t = 18$. The image at $t = 23$ using the mean subtraction method has much more clutter, which is further elucidated by the mesh plots.

5. SUMMARY

This paper presents novel approaches to antenna and air-to-ground deembedding in connection with SF-GPR. The antenna deembedding is based on antenna response deconvolution. The antenna response is determined using waveguide field theory and measurements of characteristic parameters. Successful antenna deembedding is important resolution enhancement and for subsequent mine detection methods. Air-to-ground deembedding is based on SVD/PCA analysis of the assembly of SF-GPR signals within a certain xy-area. The PCA based method is able to display similarities and differences among the signals within the area, thus the air-to-ground interface reflection is mainly present in a few principal components. Omitting these components in the subsequent reconstruction of the signals enables promising air-to-ground suppression and clutter reduction. Future studies will involve automatic selection of principal components to be retrained, as well as related techniques, e.g., ndependent components analysis[3] (ICA). The belief is that ICA would produce even more peaked components, providing better separation between the air-to-ground reflection, reflections from mines, and from clutter. In addition, we plan to use the PCA based features as input to nonlinear statistical supervised detection algorithms.

Acknowledgements

JL is supported by the Danish Research Councils through the THOR Center for Neuroinformatics. BK acknowledge the Siemens Foundation for financial support. The authors would like to thank Anders Friedmann and Anders Gustafson for valuable comments and suggestions in connection with the field test measurements. Furthermore, Ole Nymann is acknowledged for enthusiastic and steady support of our work in humanitarian mine detection.

REFERENCES

1. D.J. Daniels: *Surface Penetrating Radar*, IEE, Radar, Sonar, Navigation and Avionics Series 6, 1996.
2. L.K. Hansen, J. Larsen, F.Å. Nielsen, S.C. Strother, E. Rostrup, R. Savoy, N. Lange, J. Sidtis, C. Svarer & O.B. Paulson: *et al.*: "Generalizable Pattern in Neuroimaging: How Many Principal Components?," *NeuroImage*, vol. 9, pp. 534–544, 1999.
3. L.K. Hansen, J. Larsen & T. Kolenda "On Independent Component Analysis for Multimedia Signals," in L. Guan, S.Y. Kung and J. Larsen (eds.) *Multimedia Image and Video Processing*, CRC Press, 2000, to appear.
4. J.E. Jackson: *A Users Guide to Pricipal Components*, New York: John Wiley and Sons Inc., 1991.
5. B. Lautrup, L.K. Hansen I. Law, N. Mørch, C. Svarer, S.C. Strother: "Massive weight sharing: A Cure for Extremely Ill-posed Problems," in H.J. Herman *et al.*, (eds.) *Supercomputing in Brain Research: From Tomography to Neural Networks*, World Scientific Pub. Corp. pp. 137–148, 1995.
6. J.G. Proakis & D.G. Manolakis: *Digital Signal Processing*, Ney Jersey: Prentice Hall, 3rd edition, 1996.
7. S. Ramo, J.R. Whinnery, T.V. Duzer: *Fields and Waves in Communication Electronics*, 3rd ed., New York: John Wiley and Sons Inc., 1994.
8. W.L. Stutzman, G.A. Thiele: *Antenna Theory and Design*, 2nd ed., New York: John Wiley and Sons Inc., 1998.
9. A.D. Yaghijan: "Approximate Formulas for the Far Field And Gain of Open-Ended Rectangular Waveguide," *IEEE Transactions on Antennas and Propagation*, vol. AP-32, no. 4, April 1999.
10. S.H. Yu & T.R. Witten: "Automatic Mine Detection based on Ground Penetratinig Radar," *SPIE Conference on Detection and Remediation Technologies for Mines and Minelike Targets IV*, Orlando, Florida, vol. 3710, pp. 961–972, 1999.